Digital holographic microscopy real-time monitoring of cytoarchitectural alterations during simulated microgravity

Christophe Pache
Ecole Polytechnique Fédérale de Lausanne
Advanced Photonics Laboratory
Lausanne, 1015 Switzerland
and
Eidgenössische Technische Hochschule Zürich
Space Biology Group
Zürich, 8005 Switzerland

Jonas Kühn
Ecole Polytechnique Fédérale de Lausanne
Advanced Photonics Laboratory
Lausanne, 1015 Switzerland
and
University Hospital of Vaud
DP-CHUV
Prilly s/Lausanne, 1008 Switzerland

Kriss Westphal
Eidgenössische Technische Hochschule Zürich
Space Biology Group
Zürich, 8005 Switzerland

M. Fatih Toy
Jérôme Parent
Ecole Polytechnique Fédérale de Lausanne
Advanced Photonics Laboratory
Lausanne, 1015 Switzerland

Oralea Büchi
Alfredo Franco-Obregón
Eidgenössische Technische Hochschule Zürich
Institute of Biomedical Engineering
Mechanobiology Laboratory
Zürich, 8005 Switzerland

Christian Depeursinge
Ecole Polytechnique Fédérale de Lausanne
Advanced Photonics Laboratory
Lausanne, 1015 Switzerland

Marcel Egli
Eidgenössische Technische Hochschule Zürich
Space Biology Group
Zürich, 8005 Switzerland

Abstract. Previous investigations on mammalian cells have shown that microgravity, either that experienced in space, or simulated on earth, causes severe cellular modifications that compromise tissue determination and function. The aim of this study is to investigate, in real time, the morphological changes undergone by cells experiencing simulated microgravity by using digital holographic microscopy (DHM). DHM analysis of living mouse myoblasts (C2C12) is undertaken under simulated microgravity with a random positioning machine. The DHM analysis reveals cytoskeletal alterations similar to those previously reported with conventional methods, and in agreement with conventional brightfield fluorescence microscopy *a posteriori* investigation. Indeed, DHM is shown to be able to noninvasively and quantitatively detect changes in actin reticular formation, as well as actin distribution, in living unstained samples. Such results were previously only obtainable with the use of labeled probes in conjunction with conventional fluorescence microscopy, with all the classically described limitations in terms of bias, bleaching, and temporal resolution.
[DOI: 10.1117/1.3377960]

Keywords: microgravity; muscle cells; mechanobiology; cell morphology; actin cytoskeleton; digital holography; quantitative phase imaging; microscopy.

Paper 09562R received Dec. 18, 2009; revised manuscript received Feb. 25, 2010; accepted for publication Feb. 26, 2010; published online Apr. 6, 2010.

1 Introduction

The cytoskeleton is involved in a variety of core cellular functions, including shape determination, mechanical support, and the multidirectional traffic of biosynthetic organelles within the cytoplasmic compartment. Cytoskeleton dynamics are hence necessary for cell viability, perpetuation, and differentiation.[1,2] The three basic cytoskeletal filaments in mammalian cells, microtubules, intermediate filaments, and actin microfilaments, are principally involved in subcellular organization, structural support, and interactive cell behavior, respectively.

A growing body of research is now demonstrating that gravitational forces influence cytoskeletal dynamics in mammalian cells.[2–4] The extent to which the cytoskeleton of mam-

Address all correspondence to: Christophe Pache, Ecole Polytechnique Fédérale de Lausanne, Advanced Photonics Laboratory, Lausanne, 1015 Switzerland. Tel: 41-21-6937773; Fax: 41-21-6933701; E-mail: christophe.pache@epfl.ch

1083-3668/2010/15(2)/026021/9/$25.00 © 2010 SPIE

malian cells responds to microgravity (μg), however, varies with cell type and the method whereby microgravity is established. Erythroleukaemic cells (Friend cells) cultivated for 6 days in the ESA Biorack facility during the IML-1 mission exhibited minor differences in mean cell volume or mitotic index between 0 and 1 g (onboard 1 g centrifuge).[5] By contrast, lymphatic cells (Jurkat cells and human T-cells) showed significant modifications of the cytoskeleton after a sounding rocket or space shuttle flight; vimentin collected into large bundles after only 30 s in 0 g.[6,7] Dramatic reorganizations of the microtubular matrix and increased apoptotic entry were also apparent.[1] Cultured glial cells (C6 cell line) experiencing simulated microgravity on the random positioning machine (RPM) showed severe cytoskeletal rearrangements after 15–30 min. Microfilaments and intermediate filaments became highly disorganized, microtubules lost their radial array and the overall cellular shape deteriorated.[8] Surprisingly, most of the cells recovered from continuous microgravity simulation after ~20 h.[8]

Because the developmental programs of bones and muscle are exquisitely sensitive to mechanical input, myoblasts and osteoblasts are particularly responsive to changes in gravitational force. Studies conducted onboard the space shuttle demonstrated that osteoblasts undergo changes in morphology at 0 g.[9] Other studies on osteoblastic cells similarly showed a mixture of altered cell morphologies including an increased incidence of rounded cells at 0 g.[10] Relatively fewer studies have focused on the cytoskeletal alterations of muscle cells in response to mechanical unloading as a result of reduced gravitational forces. L8 rat myoblasts failed to differentiate and fuse into myotubes after space shuttle flight.[11]

Gravitational forces strongly influences actin cytoskeletal dynamics.[12] The actin cytoskeletal network plays a key role in cell fate determination in response to mechanical and/or humoral stimuli because it regulates the transition through the developmental programs of most progenitor cell classes. In muscle cells, the actin cytoskeleton mediates cell-cell separation (cytokinesis) during the proliferative phase of myogenesis as well as initiates cell-cell fusion during myogenic differentiation.[13] The actin cytoskeleton achieves this dichotomous feat by monitoring and responding to the adhesive forces originating from the extracellular matrix, or neighboring cells, and next converting these forces into a genetic response.[14] The actin cytoskeletal network thus controls the transit of myoblasts from cell division to cell fusion by titrating mechanical signals arising from the extracellular environment. Surprisingly, the effect of microgravity over the actin cytoskeletal network of mammalian myogenic progenitor cells is relatively unstudied.[4]

A variety of platforms have been used to either simulate, or exploit, existing states of microgravity including clinostats, RPMs, parabolic flights, sounding rockets, or orbiting spacecrafts, such as space shuttles.[1] Although these studies have clearly shown that microgravity-induced rearrangements of the cytoskeleton are highly dynamic, their interpretation is hampered by the fact that they rely on the extrapolation of information from a time series of static "snapshots" of cell behavior, an approach that cannot fully reveal the highly choreographed series of events leading up to cytoskeleton reorganization in response to microgravity, and hence, valuable information about the underlying mechanisms is inevitably lost. To gain broader insights into these dynamic processes, real-time quantitative assessments of cytoskeletal kinetics under microgravity are needed.

Real-time analysis of cell changes can be achieved with digital holographic microscopy (DHM).[15–21] This novel interferometric microscopy technique provides quantitative phase images[22,23] with nanometer-range accuracy,[24] that are directly related to the optical path length (OPL) induced by the sample. This OPL parameter, also called "optical thickness," is both proportional to the intracellular refractive index, linked to cellular content, and absolute cytomorphological topography.[16,17] Moreover, DHM measurements are strictly noninvasive, label free, and far below the phototoxicity optical power threshold. The DHM technology can also provide so-called digital focusing, resulting in an extended depth of field,[25] and camera acquisition times in the microsecond regime grant DHM with an excellent robustness regarding environmental disturbances, such as vibrations or shocks. All the previous features potentially make DHM an ideal microscopic tool for real-time monitoring of living cells under harsh conditions onboard a fast-moving RPM.

The study of cytoskeletal dynamics in response to distinct mechanical environments is of broad clinical importance. Essential cell behaviors, such as proliferation, differentiation, or apoptosis, elicit strictly choreographed changes in the cytoskeletal network that are influenced by mechanical input. Prominent among the mechanical stimuli that are known to regulate cell determination are gravitational forces. An understanding of the underlying mechanisms involved in cellular mechanotransduction will thus provide important insights into complex tissue development, as well as open the way for more effective therapeutic interventions aimed at improving tissue regeneration following trauma or disease.

The aim of this study was to monitor the cytoarchitectural changes of mouse C2C12 myoblasts under microgravity by DHM in real time, and compare the results to established brightfield fluorescence microscopy measurements. As previously mentioned, microgravity was simulated with a RPM, allowing for live monitoring of cellular changes during the transition from 1 to 0 g and then during constant microgravity exposure in time. A custom-developed DHM setup has been realized to fit onto a RPM, while being remotely operated on the moving platform. The real-time DHM measurements are then *a posteriori* compared to snapshot (time samples) results on fixed cells obtained by fluorescence microscopy.

2 Materials and Methods

2.1 *DHM*

DHM[26–30] is an innovative interferometric microscopy technology enabling complete complex optical wavefront retrieval from a specimen, illuminated either in reflection or in transmission. The working principle relies on the acquisition of a hologram, generated by the interference between a so-called object wave (O) and a reference wave (R), by a digital camera, such as a charge-coupled device (CCD). Thereafter, the complex wavefront in the acquisition plane can be entirely retrieved by software processing,[31–34] both in amplitude and

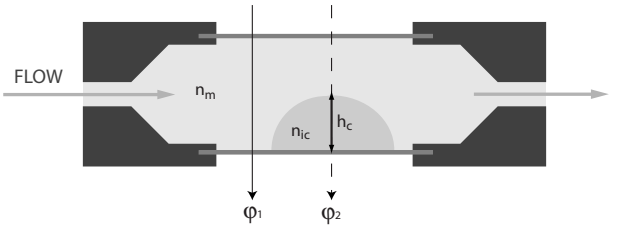

Fig. 1 Schematic of the usual transmission DHM sample configuration with a closed or open perfusion chamber, and the corresponding measured phase signals φ_i with $i=1,2$. n_m, culture medium refractive; n_{ic}, mean intracellular refractive index; h_c, cellular thickness.

noticeably in quantitative phase,[22,23] and eventually digitally propagated to the in-focus plane by common Fresnel, convolution, or angular spectrum algorithms.[28,30,35]

Thanks to its noninvasive and noncontact nature, DHM has already been widely applied in transmission configuration to investigate transparent samples in real-time, mostly regarding life sciences applications under 1-g laboratory conditions, like monitoring neurons under hypotonic stress,[17] red blood cells,[21] cancerous cells,[18,19] dynamic cytoskeletons changes,[20] or cell-division dry mass evolution.[36] In transmission, the measured quantitative phase signal φ is linked to the so-called integrated OPL (i.e., the optical thickness) through the sample as in

$$\varphi(x,y) = 2\pi\frac{\mathrm{OPL}(x,y)}{\lambda} \quad \text{with} \quad \mathrm{OPL}(x,y) = \int_z n(x,y,z)dz, \tag{1}$$

where x, y are the coordinates of the considered pixel in the phase map, z the vertical coordinate along the optical axis, λ the light wavelength, and n the refractive index at a given position inside the sample volume.

The study of living cells often requires their submergence in culture medium either inside a closed immersion or open perfusion chamber as illustrated in Fig. 1. In such a configuration, the measured phase data correspond to the phase difference $\Delta\varphi$ between φ_1 and φ_2 (see Fig. 1) as expressed in Eq. (2), where it is proportional to the refractive index mismatch between the sample and the immersion medium

$$\Delta\varphi(x,y) = \varphi_2 - \varphi_1 = \frac{2\pi}{\lambda}[\overline{n_{ic}}(x,y) - n_m]h_c(x,y), \tag{2}$$

where n_{ic} is the mean intracellular refractive index, n_m the surrounding medium refractive index, and h_c the sample thickness (i.e., the absolute topography in case of complete adherence on the surface on one side).

As can be observed in Eq. (2), the DHM-measured phase information gives rich insights about both intracellular refractive index, proportional to intracellular content density (water, proteins, etc.), and the actual cytomorphology. It is typical to reach 3×10^{-4} precision on refractive index and about 10-nm axial accuracy with transmission DHM,[17] thanks to the interferometric precision of the technique. The lateral resolution remains diffraction limited by the microscopy-objective (MO) numerical aperture (NA), as in classical microscopy. If needed, so-called decoupling procedures to independently retrieve both refractive index and topographical values from the phase measurement exist using for instance, sequential culture medium exchange,[17] fixed chamber channel height squeezing the cells,[19] or recently true real-time decoupling by dual wavelength using dispersion with a dye-enhanced surrounding medium.[37][ME1]

2.2 *DHM Setup*

The RPM-DHM prototype used in this study was a transmission setup based on a Mach–Zehnder interferometer configuration, as depicted in Fig. 2(a). The laser source was a 650-nm wavelength semiconductor laser diode with an optical output power of 1 mW, with a coherence length of $\sim$300 μm. Briefly, at first the beam was collimated and divided by a first beamsplitter (BS) into two interferometer arms, the object wave O, and the reference wave R. A neutral density filter (NF) was inserted into the object arm to balance the intensity ratio between the arms. A condenser lens focuses the object beam onto the sample, where diffracted light was collected by a 60×0.85 NA MO to be recombined with the reference wave in off-axis configuration (slight angle between the propagation vectors) generating the hologram recorded by a digital CCD camera (Basler A101f, Basler Vision Technologies, Ahrensburg, Germany). The delay line (DL) in the reference arm was designed to match the OPL of both arms in order to get interferences with the reduced coherence length.

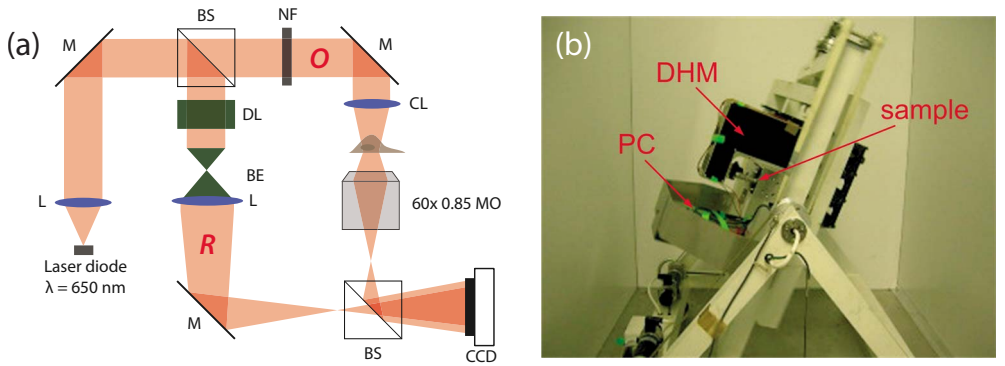

Fig. 2 Custom-designed transmission DHM for the RPM: (a) Optical setup. M, mirror; L, lens; BS; NF BE; O, object wave; R, reference wave; DL; CL, condenser lens; and MO. (b) Actual experimental microgravity configuration, with the DHM mounted on the inner frame of the RPM and a built-in minicomputer fixed to the platform as well, partially counterbalancing the weight of the DHM.

The use of low temporal coherence light discards most parasitic interferences contributions and enables it to reach a single-shot axial accuracy in phase of roughly 2–3 deg. The reference beam was then spatially filtered and expanded within the beam-expander (BE) section.

Given the harsh experimental conditions onto the RPM, it is clear that the use of a dry-configuration MO was mandatory. Indeed, although the reachable resolution is theoretically better with high-NA oil-immersion MOs, the platform for the DHM on the RPM was obviously going to continuously rotate, which prevented using immersion oil or any other liquid. The retained microscopy option was therefore a dry-configuration 60×0.85 NA MO, providing a field-of-view of about 65×65 μm^2 on a 512×512 pixels region of interest on the CCD camera, with a lateral resolution in the 500-nm range.

A built-in minicomputer integrated in the DHM was in charge of controlling the camera acquisition parameters, as well as to acquire and store the recorded holograms during the experiment. The onboard computer was configured with a low-consumption CPU (Intel Core Soleo 1 GHz; SDRAM 667 MHz) and a compact flash memory of 8 GB at 20 MB/s, enabling a theoretical recording rate of 78 images/second for 512×512 pixels holograms (the used CCD camera was limited to 25 images/second). However such a high frame rate was not necessary for the experiments, and effective framerate for both 1-g control and microgravity recorded holograms was chosen as 1 image/second. At the end of experimental sessions, all locally stored data was uploaded to an external workstation for hologram reconstruction and all experimental data postprocessing. Hologram file size was set to 512×512 pixels, recorded in 8-bit TIFF format. An overview of the actual experimental configurations onboard the RPM is depicted in Fig. 2(b). It is important to note that the DHM position on the RPM platform was designed so that the sample position was exactly located at the RPM rotation center, in order to fulfill microgravity conditions for the specimen and eliminate centrifugal acceleration. Finally, the DHM-investigated C2C12 cells were cultivated at 37°C in special custom-designed flasks (μ-slide I, Ibidi GmbH, Munich, Germany), which purposely had the same thickness as standard coverslips (0.17 mm).

2.3 *Random Positioning Machine (RPM)*

The RPM or three-dimensional clinostat is a laboratory instrument to simulate microgravity condition. Originally, the machine was developed by Hoson et al.[38] and manufactured by Dutch Space, Leiden, The Netherlands. Samples mounted on a platform randomly change the position in the 3-D space on the machine, controlled by dedicated software running on a personal computer. The movement of the experimental platform suspended in the center of two cardanic frames is realized by two independently running engines. These engines are controlled by feedback signals from encoders mounted on the motor axes. The RPM was operated as 3-D clinostat in a random walk (basic mode) with a rotation speed of 60 deg/s in a temperature controlled room (37 ± 1 °C).

2.4 *Fluorescence Microscopy Investigations on Cells Exposed to Microgravity*

As already mentioned, all experiments were carried out on actin-GFP transfected C2C12 mouse myoblasts. Thus, actin filament structures were visible under fluorescence microscope (blue excitation, green emission) without additional labeling. The C2C12 cells were myogenic progenitor cells, capable of differentiating into myotubes *in vitro* on serum withdrawal.[39] The fusion of myoblasts with existing myotubes is what gives rise to the adult skeletal muscle fibers observed in the animal.[40,41]

C2C12 myoblast cells were cultured in an incubator at 37 °C, 5% CO_2 in RPMI 1640 (Cellgro, Mediatech, Inc., Manassas, Virginia) supplemented with 10% fetal calf serum (PAA, Cölbe, Germany), 1% penicillin/streptomycin (PAA, Cölbe, Germany), and 0.6% geneticin (GIBCO, Auckland, New Zealand). Antibiotic treatment ensures that only GFP-tagged cells are cultivated because they also express the antibiotic resistance. This way, a loss of fluorescent signal can be reduced. The cells were fed twice a week. Before seeding the cells in different cell flasks (Nunc, Roskilde, Denmark) for the investigation on the RPM, they were detached from the culture flask by exposure to 0.25% trypsin/EDTA (Invitrogen, Eggenstein, Germany) for 2 min at confluency of maximum 80%. The RPM rotation velocity was then set to 60 deg/s and sample images were taken after various time points of simulated microgravity exposure. Ground controls (1 g) were placed on the frame of the RPM in order to subject all the samples to the same temperature variations and mechanical vibrations as the microgravity samples.

Some microgravity-induced morphological and cytoskeletal change measurements under simulated microgravity were carried out on fixed cells. At particular exposure periods to microgravity and 1 g, cells were harvested and immediately fixed by 4% paraformaldehyde for 15 min before DAPI staining. The following protocol was used: 5-min incubation in Triton X-100 (0.1%) and then 5-min exposure to DAPI dye (50 ng/mL). Rinsing of the cells with phosphate buffered saline (PBS) was carried out in between all the steps described. At the end, the slides were embedded with Aqua Poly/Mount (Polysciences Inc., Warrington, Pennsylvania). Samples were observed thereafter by using an inverse epifluorescence microscope equipped with a 40×0.85 NA UplanApo MO and a 60×1.45 NA oil-immersion Ph PlanApo MO. All the fluorescence images were recorded in gray scale on both channels (DAPI and GFP filters) separately, then colored and merged together.

The perinuclear actin concentration was further investigated by extracting pixel intensity profiles from GFP images. Each profile had a fixed length of 80 pixels (which is about the diameter of a nucleus) and was drawn from the edge of the nucleus in the opposite direction. In each time series, two profiles per image were taken from different directions (at least 20 deg apart). Four cells per group (microgravity or 1 g for a specific time series) were investigated.

2.5 *Protein Content Verification Procedure*

C2C12 cells were cultured until sub-confluence had been reached. At this stage, the cells were cultured after exposure to normal and simulated microgravity conditions for 0, 5, 10,

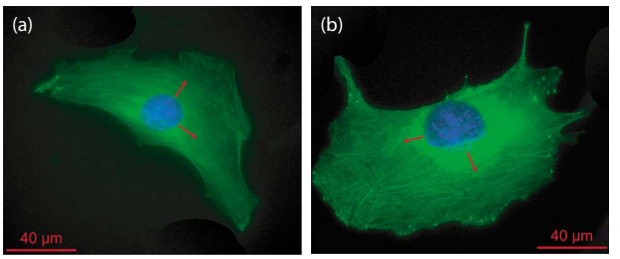

Fig. 3 Widefield images of C2C12 cells at (a) 10 min 1-g control condition, and (b) 10 min 0-g exposure, with examples of profiles (red arrows) for determination of the microgravity-induced accumulation of actin around the nucleus. (Color online only.)

30, and 60 min. Immediately afterward, the cells were trypsinised, centrifuged (1500 rpm, 5 min), washed with PBS, and centrifuged again. At the end, pellets were stored at −80 °C until further processing. For the analysis, the pellets were resuspended in lysis buffer (CellLytic-M Cell Lysis Reagent, Sigma, C2978) containing freshly done protease inhibitor cocktail (Complete Mini, Roche, ref 11 836 153 001). After a 30-min incubation period at 4 °C, insoluble cells debris were removed by centrifugation (4 °C, full speed, 30 min). Protein concentrations were determined afterwards by using the BC Assay Protein Quantification Small Kit (Uptima, UP40840B) according to manufacturer's instructions. The quantification was performed using Microplate Manager Software (measurement filter: 540 nm, mix time 5 s). BSA was used as a standard. Statistical analyses were carried out using the software SPSS (SPSS Inc., Chicago, Illinois).

3 Results

3.1 *Morphological and Cytoskeletal Changes Observation by Fluorescence Microscopy*

In comparison to control cells shown in Fig. 3(a), exposure of C2C12 cells to simulated microgravity stimulated the growth of lamellipodia as depicted by a weblike organization of the actin cytoskeleton at the mobile edge of the cell in Fig. 3(b). An increase in lamellipodial outgrowth was observed after only 10 min of exposure to microgravity. The proportion of

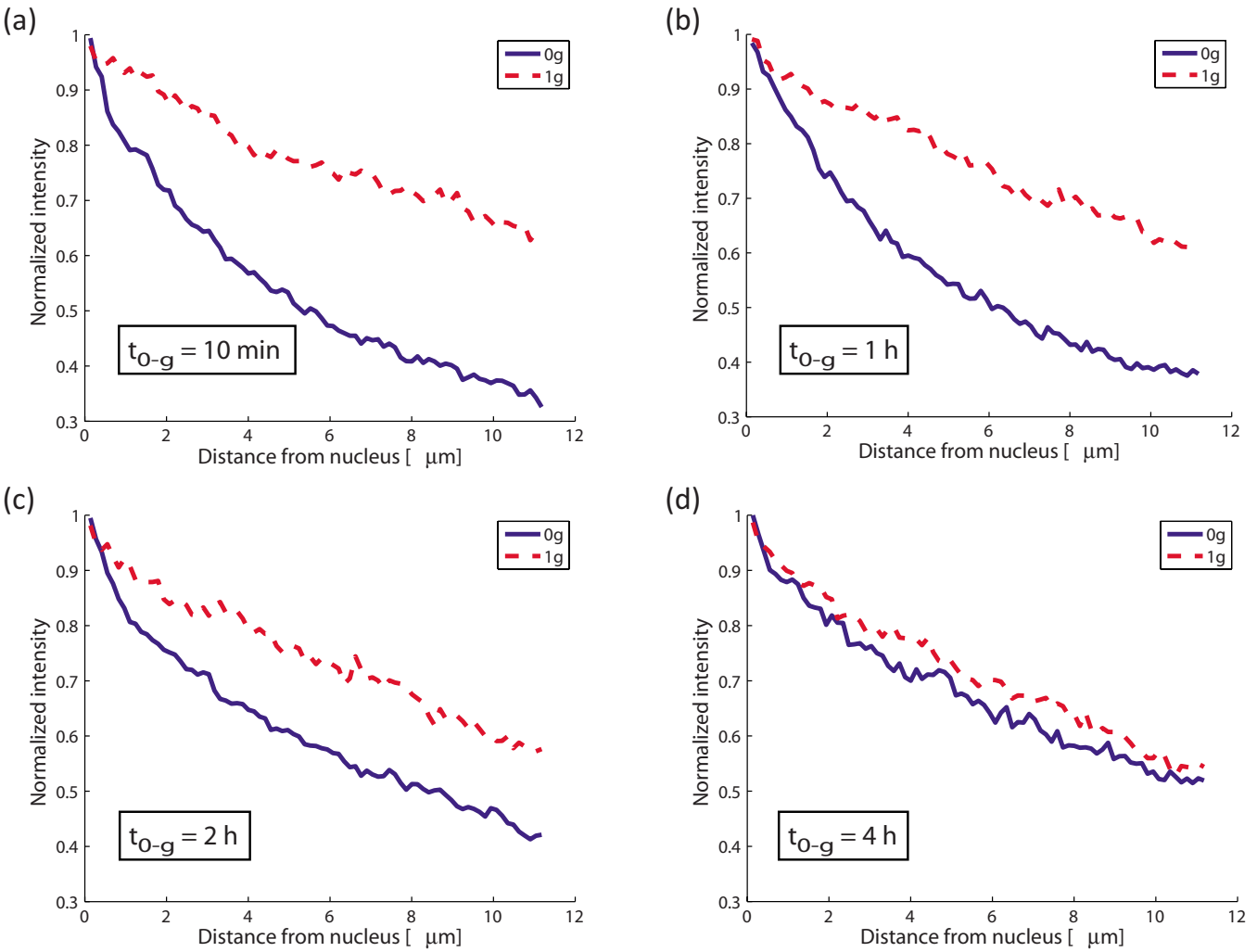

Fig. 4 Accumulation of actin around the nucleus at $t_{0\ g}$=(a) 10 min, (b) 1 h, (c) 2 h, and (d) 4 h of simulated microgravity exposure times. Significant differences between 1 and 0 g cells were detected up to 2 h (Mann–Whitney U-test) with actin distribution around the nucleus apparently adapting after 4 h.

cells exhibiting such actin cytoskeletal changes increased with time exposure to microgravity up until ~2 h, where a steady state in cell morphological changes seemed to be reached (data not shown).

In addition to lamellipodial outgrowth, the actin distribution within the soma also changed in response to simulated microgravity; stress fibers became denser and more randomly organized and nonfilamentous actin began to accumulate around the nucleus [Fig. 3(b)]. To evaluate the time course of actin accumulation around the nucleus, pixel intensity profiles were extracted and normalized to the maximum value. Two profiles were taken at different orientations (at least 20° between the two segments) as depicted by the red arrows in Fig. 3(b) at 10 min, 1 h, 2 h, and 4 h of exposure to simulated microgravity exposure. Indeed, given the time frame of fluorescent sample preparation described in Section 2.4, measurements of microgravity exposures of <10 min make little sense and risk of induced bias are high. Significant differences in perinuclear complexity were detected (The Mann-Whitney U-test) until up to 2 h, as is demonstrated in Fig. 4. The rate of decrease in actin concentration with distance from the cell nucleus was greater in 1-g control cells than in microgravity. After 10 min of exposure to simulated microgravity, the difference between the two groups (1 g and microgravity) was significant in Fig. 4(a). At 1 h, the same significance was computed for in Fig. 4(b) and after 2 h in Fig. 4(c). At longer durations (4–25 h), the cells seemed to adapt themselves and no noticeable difference was calculated as depicted in Fig. 4(d).

3.2 *In Situ DHM Monitoring of Cell Changes under Microgravity Condition*

The main purpose of using DHM was to verify if microgravity-induced changes in the cytoskeleton commonly observed by fluorescence microscopy on fixed C2C12 cells (e.g., Figs. 3 and 4) could also be detected by DHM in real time on the RPM. This could enable the investigation of the cellular mechanisms responsible for the observed dynamic changes in the cytoskeleton. In addition to this, DHM potentially provides a much finer temporal resolution to investigate quick responses to microgravity compared to fluorescence microscopy, as in Fig. 4.

Changes in perinuclear optical thickness with time at microgravity were confirmed by DHM analysis. As can be seen in Fig. 5, when compared to the epifluorescence micrograph of Fig. 3(b), the phase measurements changed immediately on exposure to microgravity. No significant changes occurred around the nucleus during the 1-g control period (8 min), whereas microgravity readily initiated cytosolic modifications. Switching on the RPM caused a continuous accumulation of proteins around the nucleus, translated into a phase increase (Fig. 5). The first apparent modifications were already detected after 2 min of exposure to microgravity and persisted to accumulate throughout the measured period of 1.5 h. The current DHM platform does not distinguish between actin or other proteins. Therefore, the series of DHM images shown in Fig. 5 represent a total accumulation process from potentially different sources. Because of technical reasons, noticeably RPM onboard power supply instability during extended operation times, DHM investigation for a period of longer than 1.5 h were not possible with this experimental prototype.

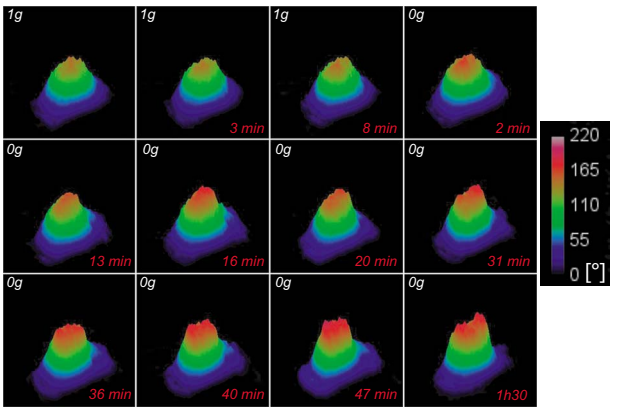

Fig. 5 DHM quantitative phase images in perspective 3-D view, showing the cell thickening process around the nucleus under simulated microgravity: Microgravity was switched on after a control period of 8 min. FOV: 51×58 μm^2.

Growth of lamellipodia under simulated microgravity conditions was also monitored with DHM, as shown in Fig. 6. During the initial test period (10 min at 1 g) no changes of leading-edge morphology or OPL were apparent. There was no detectable change in lamellipodia area, and the edges of the lamellipodia retain their interaction zone with the substrate. After switching on the RPM, on the other hand, much of the lamellipodial interactions were retracted and filopodia extended in their place. After 2 min of microgravity, the phase-shift measurement doubled in this area, as can be clearly seen in Fig. 6 time-series images. The structure continued to grow until the end of the recording period of 20 min. Obviously, the microgravity environment induced a reorganization of the cell's leading edge. These observations are in good agreement with the results obtained with the traditional fluorescence microscope (Fig. 3) in that actin was shown to organize into dense bundles at the leading edge of the cell (typical filopodial actin scaffold) when exposed to microgravity.

3.3 *Estimation of Total Protein Amount*

Epifluorescence microscopy, as well as DHM quantitative phase investigations of the C2C12 cells under simulated microgravity, reveals substantial changes of cell morphology in

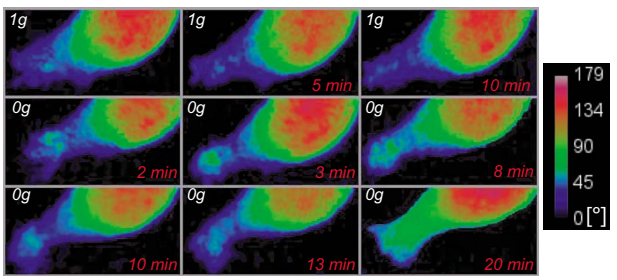

Fig. 6 Quantitative phase images of the evolution of lamellipodium growth initiated by simulated microgravity, monitored in real time by DHM. Vertical scale in degrees, FOV: 32×16 μm^2.

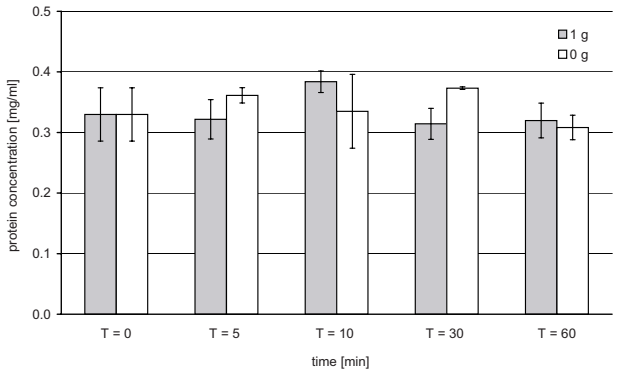

Fig. 7 Total protein amount of C2C12 cells under control (1 g, gray) and simulated microgravity conditions (0 g, white), indicating that no differences between the two different conditions are detected, even after 60 min. Values are expressed as mean protein concentration ± SD.

comparison to the 1-g control group. These changes occur mainly within the first hour of microgravity exposure. In order to verify whether the changes are due to reorganization or *de novo* synthesis of cytoskeletal proteins, it is useful to measure the total amount of proteins after normal 1-g and microgravity exposure. The protein content of C2C12 are determined after 5, 10, 30, and 60 min. As plotted in Fig. 7, analysis of the probes reveal no statistically significant difference between all the different groups.

4 Conclusions

Our RPM-compatible DHM experimental setup allows a comprehensive and quantitative real-time analysis of living cells dynamic behavior during exposure to simulated microgravity, and this *in situ*. The proposed DHM system is granted with sufficient robustness to achieve live interferometric measurement onboard a RPM platform at 60 deg/s, not only demonstrating single-shot DHM inherent advantage regarding vibration management, but also paving the way for future microgravity studies on different platforms, such as parabolic or even spaceflights. In this regard, the early-days DHM technology already proved to hold a remarkable potential for space applications, even on the International Space Station.[42,43] To our knowledge, the presented results are the first-phase images of living cells undergoing dynamic cytoarchitectural modifications to simulated microgravity for an extended period. As demonstrated in this paper, DHM provides data about cytoarchitecture changes that were previously only available from *a posteriori* observation of chemically fixed samples by fluorescence microscopy. Further technical improvements will attempt to extend DHM monitoring time to several hours, to get the same time spanlike fluorescence microscopy, but with the finer temporal sampling provided by the real-time feature. For example, this upgrade could interestingly enable to verify if the actin concentration behavior after 4 h measured by fluorescence in Fig. 4(d) can also be observed by DHM. In addition to this, future works will also be aimed at relating the quantitative phase measurement provided by DHM to true physical data, in term of absolute cytomorphological topography and intracellular refractive index, possibly by using decoupling procedures[17,37] or validating hypothesis of either negligible refractive index or volume change. Such an advance will further reinforce the potential of DHM for the understanding of intracellular modifications dynamics when cells are exposed to microgravity.

In the exposed experimental results, living C2C12 myoblasts show two principal modifications while experiencing simulated microgravity: (*i*) a retraction of existing lamellipodia with consequent reorganization of the actin cytoskeletal network into filopodial-like contacts with the substrate and, (*ii*) more uniquely, a perinuclear accumulation of actin presumably coincident with the collapse of the cell reticular formation around the nucleus. Both these effects could be explained by changes in the regulatory mechanisms of the actin cytoskeleton. Many cell types undergo profound cytoskeletal alterations in response to changes in gravitational force.[4] The actin cytoskeleton is a key instigator of many of these changes because it is intimately involved in translating mechanical stimuli into biochemical responses. Moreover, because mechanical input controls the developmental programs of the body's structural tissues, the loss of gravitational force will compromise the development of the greater part of our total body tissue, particularly bones and muscles. For instance, the withdrawal of myoblasts from the cell cycle and their subsequent commitment to terminal differentiation is a response to mechanical input that relies on the reorganization of the actin cytoskeleton at the cell periphery.[13,44] Myoblast proliferation and differentiation are facilitated by lamellipodia and filopodia, respectively, that are under the control of Rac1 and Cdc42 actin-regulating GTPases, respectively.[45,46] We now have preliminary data demonstrating that myoblasts experiencing simulated microgravity withdraw from the cell cycle earlier than normal (at a lower cell density) and prematurely differentiate, a result that is consistent with the finding of Fig. 2 that myoblasts under microgravity retract lamellipodial contacts with the substrate. Our results indicate that the loss of gravitational force upsets the normal expression pattern of the distinct Rho GTPases effectively short-circuiting muscle development as a result of insufficient expansion of the myoblast pool and precocious differentiation. At the cytoskeleton level, these effects are manifested as a retraction of existing lamellipodia and the fortification of filopodia, possibly as a result of increased Cdc42 expression and indicative of a cellular state of reduced cell migration and proliferation.

Additionally, Cdc42 regulates membrane traffic between the golgi apparatus and endoplasmic reticulum, where it has been shown to nucleate actin filaments onto retrograde transport vesicles.[45,47,48] Although the role that actin plays in golgi vesicular traffic remains to be fully appreciated, overexpression of Cdc42 inhibits retrograde membrane transport from the golgi apparatus to endoplasmic reticulum as well as coalesces the golgi apparatus tightly around the nucleus.[47,48] It is intriguing to postulate that microgravity promotes the expression of Cdc42, nucleating actin onto vesicles *en route* to the endoplasmic reticulum from the golgi apparatus and causing their retention in the perinuclear region. Such an effect would explain the specific accumulation of actin in the perinuclear space shown in Fig. 3. The possibility that Cdc42 expression is upregulated in response to microgravity will be corroborated by the demonstration that the cell reticular formation collapses into more proximal perinuclear regions in myoblasts exposed to microgravity.

In closing, we have demonstrated that the DHM is able to noninvasively and quantitatively detect subtle changes in cytoskeletal organization in living samples without the use of fluorescently conjugated probes of common use in conventional fluorescence microscopy. The implications of this novel utility of the DHM to cell biological research are profound.

References

1. N. I. Lewis, W. Xu, S. K. Jericho, H. J. Kreuzer, M. H. Jericho, and A. D. Cembella, "Swimming speed of three species of Alexandrium (Dinophyceae) as determined by digital in-line holography," *Phycologia* **45**, 61–70 (2006).
2. M. Hughes-Fulford, "Function of the cytoskeleton in gravisensing during spaceflight," *Adv. Space Res.* **32**, 1585–1593 (2003).
3. R. H. Fitts, D. R. Riley, and J. J. Widrick, "Microgravity and skeletal muscle," *J. Appl. Physiol.* **89**, 823–839 (2000).
4. S. J. Crawford-Young, "Effects of microgravity on cell cytoskeleton and embryogenesis," *Int. J. Dev. Biol.* **50**, 183–191 (2006).
5. B. Bechler, E. Hunzinger, O. Muller, and A. Cogoli, "Culture of hybridoma and Friend leukemia virus transformed cells in microgravity. Spacelab IML-1 mission," *Biol. Cell* **79**, 45–50 (1993).
6. H. Schatten, M. L. Lewis, and A. Chakrabarti, "Spaceflight and clinorotation cause cytoskeleton and mitochondria changes and increases in apoptosis in cultured cells," *Acta Astronaut.* **49**, 399–418 (2001).
7. L. Sciola, M. Cogoli-Greuter, A. Cogoli, A. Spano, and P. Pippia, "Influence of microgravity on mitogen binding and cytoskeleton in Jurkat cells," *Adv. Space Res.* **24**, 801–805 (1999).
8. B. M. Uva, M. A. Masini, M. Sturla, F. Bruzzone, M. Giuliani, G. Tagliafierro, and F. Strollo, "Microgravity-induced apoptosis in cultured glial cells," *Eur. J. Histochem.* **46**, 209–214 (2002).
9. S. A. Harris, M. Zhang, L. S. Kidder, G. L. Evans, T. C. Spelsberg, and R. T. Turner, "Effects of orbital spaceflight on human osteoblastic cell physiology and gene expression," *Bone* **26**, 325–331 (2000).
10. M. Hughes-Fulford, R. Tjandrawinata, J. Fitzgerald, K. Gasuad, and V. Gilbertson, "Effects of microgravity on osteoblast growth," *Gravit. Space Biol. Bull.* **11**, 51–60 (1998).
11. D. A. Kulesh, L. H. Anderson, B. Wilson, E. J. Otis, D. M. Elgin, M. J. Barker, W. J. Mehm, and G. P. Kearney, "Space shuttle flight (STS-45) of L8 myoblast cells results in the isolation of a nonfusing cell line variant," *J. Cell. Biochem.* **55**, 530–544 (1994).
12. D. Ingber, "How cells (might) sense microgravity," *FASEB J.* **13**(Suppl), S3–15 (1999).
13. B. Städler, T. Blättler, and A. Franco-Obregon, "Time-lapse imaging of *in vitro* myogenesis using atomic force microscopy," *J. Microsc.* **237**, 63–69 (2010).
14. A. Katsumi, A. W. Orr, E. Tzima, and M. A. Schwartz, "Integrins in mechanotransduction," *J. Biol. Chem.* **279**, 12001–12004 (2004).
15. W. Xu, M. H. Jericho, I. A. Meinertzhagendagger, and H. J. Kreuzer, "Digital in-line holography for biological applications," *Proc. Natl. Acad. Sci. U.S.A.* **98**, 11301–11305 (2001).
16. P. Marquet, B. Rappaz, P. J. Magistretti, E. Cuche, Y. Emery, T. Colomb, and C. Depeursinge, "Digital holographic microscopy: a noninvasive contrast imaging technique allowing quantitative visualization of living cells with subwavelength axial accuracy," *Opt. Lett.* **30**, 468–470 (2005).
17. B. Rappaz, P. Marquet, E. Cuche, Y. Emery, C. Depeursinge, and P. J. Magistretti, "Measurement of the integral refractive index and dynamic cell morphometry of living cells with digital holographic microscopy," *Opt. Express* **13**, 9361–9373 (2005).
18. F. Dubois, C. Yourassowsky, O. Monnom, J. C. Legros, O. Debeir, P. Van Ham, R. Kiss, and C. Decaestecker, "Digital holographic microscopy for the three-dimensional dynamic analysis of *in vitro* cancer cell migration," *J. Biomed. Opt.* **11**, 054032 (2006).
19. B. Kemper, D. Carl, J. Schnekenburger, I. Bredebusch, M. Schafer, W. Domschke, and G. von Bally, "Investigation of living pancreas tumor cells by digital holographic microscopy," *J. Biomed. Opt.* **11**, 034005 (2006).
20. J. Schnekenburger, I. Bredebusch, W. Domschke, B. Kemper, P. Langehanenberg, and G. von Bally, "Digital holographic imaging of dynamic cytoskeleton changes," *Med. Laser Appl.* **22**, 165–172 (2007).
21. B. Rappaz, A. Barbul, Y. Emery, R. Korenstein, C. Depeursinge, P. J. Magistretti, and P. Marquet, "Comparative study of human erythrocytes by digital holographic microscopy, confocal microscopy, and impedance volume analyzer," *Cytometry Part A* **73a**, 895–903 (2008).
22. U. Schnars, "Direct phase determination in hologram interferometry with use of digitally recorded holograms," *J. Opt. Soc. Am. A* **11**, 2011–2015 (1994).
23. E. Cuche, F. Bevilacqua, and C. Depeursinge, "Digital holography for quantitative phase-contrast imaging," *Opt. Lett.* **24**, 291–293 (1999).
24. J. Kühn, F. Charrière, T. Colomb, E. Cuche, F. Montfort, Y. Emery, P. Marquet, and C. Depeursinge, "Axial sub-nanometer accuracy in digital holographic microscopy," *Meas. Sci. Technol.* **19**, 074007–074008 (2008).
25. P. Ferraro, S. Grilli, D. Alfieri, S. D. Nicola, A. Finizio, G. Pierattini, B. Javidi, G. Coppola, and V. Striano, "Extended focused image in microscopy by digital Holography," *Opt. Express* **13**, 6738–6749 (2005).
26. U. Schnars, and W. Jüptner, "Direct Recording of Holograms by a CCD Target and numerical reconstruction," *Appl. Opt.* **33**, 179–181 (1994).
27. G. Pedrini, P. Froning, H. Fessler, and H. J. Tiziani, "In-line digital holographic interferometry," *Appl. Opt.* **37**, 6262–6269 (1998).
28. E. Cuche, P. Marquet, and C. Depeursinge, "Simultaneous amplitude-contrast and quantitative phase-contrast microscopy by numerical reconstruction of Fresnel off-axis holograms," *Appl. Opt.* **38**, 6994–7001 (1999).
29. S. Grilli, P. Ferraro, S. De Nicola, A. Finizio, G. Pierattini, and R. Meucci, "Whole optical wavefields reconstruction by digital holography," *Opt. Express* **9**, 294–302 (2001).
30. U. Schnars and W. P. O. Juptner, "Digital recording and numerical reconstruction of holograms," *Meas. Sci. Technol.* **13**, R85–R101 (2002).
31. T. Colomb, E. Cuche, F. Charrière, J. Kühn, N. Aspert, F. Montfort, P. Marquet, and C. Depeursinge, "Automatic procedure for aberration compensation in digital holographic microscopy and applications to specimen shape compensation," *Appl. Opt.* **45**, 851–863 (2006).
32. P. Ferraro, S. De Nicola, A. Finizio, G. Coppola, S. Grilli, C. Magro, and G. Pierattini, "Compensation of the inherent wave front curvature in digital holographic coherent microscopy for quantitative phase-contrast imaging," *Appl. Opt.* **42**, 1938–1946 (2003).
33. L. Miccio, D. Alfieri, S. Grilli, P. Ferraro, A. Finizio, L. De Petrocellis, and S. D. Nicola, "Direct full compensation of the aberrations in quantitative phase microscopy of thin objects by a single digital hologram," *Appl. Phys. Lett.* **90**, 041104 (2007).
34. P. Ferraro, D. Alferi, S. D. Nicola, L. D. Petrocellis, A. Finizio, and G. Pierattini, "Quantitative phase-contrast microscopy by a lateral shear approach to digital holographic image reconstruction," *Opt. Lett.* **31**, 1405–1407 (2006).
35. S. de Nicola, A. Finizio, G. Pierattini, P. Ferraro, and D. Alfieri, "Angular spectrum method with correction of anamorphism for numerical reconstruction of digital holograms on tilted planes," *Opt. Express* **13**, 9935–9940 (2005).
36. B. Rappaz, E. Cano, T. Colomb, J. Kuhn, C. Depeursinge, V. Simanis, P. J. Magistretti, and P. Marquet, "Noninvasive characterization of the fission yeast cell cycle by monitoring dry mass with digital holographic microscopy," *J. Biomed. Opt.* **14**, 034049 (2009).
37. B. Rappaz, F. Charrière, C. Depeursinge, P. J. Magistretti, and P. Marquet, "Simultaneous cell morphometry and refractive index measurement with dual-wavelength digital holographic microscopy and dye-enhanced dispersion of perfusion medium," *Opt. Lett.* **33**, 744–746 (2008).
38. T. Hoson, S. Kamisaka, Y. Masuda, and M. Yamashita, "Changes in plant growth processes under microgravity conditions simulated by a three-dimensional clinostat," *Bot. Mag.* **105**, 53–70 (1992).
39. D. Yaffe, and O. Saxel, "Serial passaging and differentiation of myogenic cells isolated from dystrophic mouse muscle," *Nature (London)* **270**, 725–727 (1977).
40. T. J. Hawke, and D. J. Gary, "Myogenic satellite cells: physiology to molecular biology," *J. Appl. Physiol.* **91**, 534–551 (2001).
41. M. J. Rennie, H. Wackerhage, E. E. Spangenburg, and F. W. Booth, "Control of the size of the human muscle mass," *Annu. Rev. Physiol.* **66**, 799–828 (2004).
42. F. Dubois, L. Joannes, O. Dupont, J. L. Dewandel, and J. C. Legros, "An integrated optical set-up for fluid-physics experiments under microgravity conditions," *Meas. Sci. Technol.* **10**, 934–945 (1999).

43. U. Schnars, K. Sommer, B. Grubert, H. J. Hartmann, and W. Juptner, "Holographic diagnostics of fluid experiments onboard the International Space Station," *Meas. Sci. Technol.* **10**, 900–903 (1999).
44. F. Comunale, M. Causeret, C. Favard, J. Cau, N. Taulet, S. Charrasse, and C. Gauthier-Rouvière, "Rac1 and RhoA GTPases have antagonistic functions during N-cadherin-dependent cell-cell contact formation in C2C12 myoblasts," *Biol. Cell* **99**, 503–517 (2007).
45. A. J. Ridley, "Rho GTPases and actin dynamics in membrane protrusions and vesicle trafficking," *Trends Cell Biol.* **16**, 522–529 (2006).
46. S. Servotte, Z. Zhang, C. A. Lambert, T. T. Giang Ho, G. Chometon, B. Eckes, T. Krieg, C. M. Lapière, B. V. Nusgens, and M. Aumailley, "Establishment of stable human fibroblast cell lines constitutively expressing active Rho-GTPases," *Protoplasma* **229**, 215–220 (2006).
47. O. B. Matas, S. Fritz, A. Luna, and G. Egea, "Membrane trafficking at the ER/Golgi interface: functional implications of RhoA and Rac1," *Eur. J. Cell Biol.* **84**, 699–707 (2005).
48. A. Luna, O. B. Matas, J. A. Martinez-Menarguez, E. Mato, J. M. Duran, J. Ballesta, M. Way, and G. Egea, "Regulation of protein transport from the golgi complex to the endoplasmic reticulum by CDC42 and N-WASP," *Mol. Biol. Cell* **13**, 866–879 (2002).